

Gravitational equal-area law and critical phenomena of cuspy black hole shadow

Shao-Wen Wei^{a,b}, Chao-Hui Wang^{a,b}, Yu-Peng Zhang^{a,b}, Yu-Xiao Liu^{a,b}, Robert B. Mann^c

^a*Lanzhou Center for Theoretical Physics, Key Laboratory of Theoretical Physics of Gansu Province,*

Key Laboratory of Quantum Theory and Applications of MoE,

Gansu Provincial Research Center for Basic Disciplines of Quantum Physics, Lanzhou University, Lanzhou 730000, China,

^b*Institute of Theoretical Physics & Research Center of Gravitation,*

School of Physical Science and Technology, Lanzhou University, Lanzhou 730000, China,

^c*Department of Physics & Astronomy, University of Waterloo, Waterloo, Ont. Canada N2L 3G1*

(Dated: January 23, 2026)

The formation of a cusp on a black hole shadow is a striking signature of physics beyond the Kerr paradigm. We demonstrate that this morphological change fundamentally alters the shadow's topology with the topological charge flipping from 1 to -1. To analyze this topological transition, we introduce a gravitational equal-area law, analogous to Maxwell's construction in thermodynamics, and identify a critical point for cusp formation. Near this point, we uncover universal behavior characterized by a critical exponent 1/2, which places this gravitational lensing system within the mean-field universality class. These results establish a new framework for testing fundamental physics of black hole shadows, reframing the search for deviations from general relativity as a targeted hunt for a distinct topological and critical phenomenon.

PACS numbers: 04.20.-q, 04.70.Bw, 04.25.dc

Introduction—The black hole shadow is a direct manifestation of spacetime curvature in the strong-field regime, providing a powerful probe for testing general relativity [1, 2]. Its size and shape, determined primarily by the black hole's mass and spin, offer a clean window into the fundamental nature of gravity [3–5].

The landmark Event Horizon Telescope observations of M87* and Sagittarius A* brought this theoretical prediction into an observational reality, confirming the predictions of general relativity and constraining the mass and spin of these supermassive objects [6, 7]. Crucially, these images also serve as a stringent test of theoretical frameworks: any deviation from the predicted Kerr shadow would be conclusive evidence for new physics, such as modified gravity, exotic compact objects, or surrounding dark matter [8–11].

Deviations from the Kerr metric, often parameterized as “hair”, can dramatically alter a black hole's shadow. The presence of matter fields like scalar or axion hair can deform the standard D-shape shadow into more complex patterns [12–14]. A particularly intriguing feature is the formation of a cusp, a sharp point on the shadow boundary. These cusps signify stable fundamental photon orbits, potentially linked to novel spacetime instabilities [15]. This phenomenon emerges in various non-Kerr scenarios, including black holes with Proca hair or those embedded in dark matter halos [16–19].

While cusps have been observed in specific models, a universal principle governing their formation has remained elusive. We reveal in this paper the fundamental principles governing cuspy shadows, using two powerful and complementary frameworks. First, through a topological analysis, we demonstrate that the presence of a cusp fundamentally alters the shadow's global topology. The Kerr shadow possesses a topological charge of +1, whereas the cuspy shadow has a charge of -1, placing

them in unequivocally distinct topological classes. Second, we reveal a deep analogy between cusp formation and thermodynamic phase transitions. The appearance of the cusp is a gravitational analogue of swallowtail behavior in the free energy, exhibiting universal critical behavior and admitting a gravitational Maxwell equal area-law construction to precisely determine the self-intersection points of the observable shadow boundary.

Cuspy black hole shadow—To explore the formation of cusps, we adopt the rotating Konoplya-Zhidenko (KZ) black hole, a well-defined non-Kerr solution characterized by its mass M , spin a , and a key deformation parameter η [20]. The shadow boundary is determined by unstable spherical photon orbits. Owing to the system's integrability, these orbits can be directly projected onto the celestial coordinates (α, β) of a distant observer [3]

$$\alpha = -r_0 \frac{p^\phi}{p^r}, \quad \beta = r_0 \frac{p^\theta}{p^r}, \quad (1)$$

where p^μ measures the projection of the four momentum of photons moving in the black hole background. For a distant observer ($r_0 \rightarrow \infty$) in the equatorial plane, these coordinates are given by [17]:

$$\alpha = \frac{6Mr^4 - 2r^5 + 5\eta r^2 + a^2(\eta - 2r^2(M + r))}{2a(M - r)r^2 - a\eta}, \quad (2)$$

$$\beta = \pm \frac{r^2 \sqrt{8a^2(2Mr^3 + 3r\eta) - (6Mr^2 - 2r^3 + 5\eta)^2}}{a(2r^2(r - M) + \eta)} \quad (3)$$

where r is the radius of the fundamental photon orbits. The deformation parameter η breaks the Kerr degeneracy, thus allowing for super-radiant spin values ($a > M$) even while an event horizon is preserved.

We fix the spin at $a/M = 2$ and use the deformation η to drive the system through a topological transition. The resulting shadow morphology is shown in Fig.

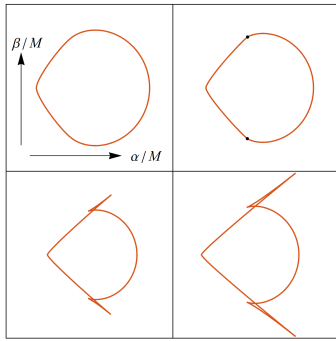


FIG. 1: Shadows cast by the KZ black hole with $a/M = 2$. The deformation parameter takes values of $\eta/M^3 = 1.5, 1.052, 0.6$, and 0.5 . Black dots denote the critical points where cusps are about to form. The bottom panels clearly show the resulting cuspy shadow structures.

1. For large values of η , the shadow is a simple closed curve, distinct from the Kerr case yet topologically equivalent. As η is lowered to a critical value of $\eta_c \approx 1.052M^3$, a pair of critical points (cusps) marked by black dots, appear on the shadow boundary. Below this threshold ($\eta < \eta_c$), the boundary develops self-intersections, forming two distinct cuspy regions that grow as η decreases. This qualitative transition from a simple closed curve to a self-intersecting one constitutes the central phenomenon studied in this paper, which we will analyze through the frameworks of topology and critical phenomena.

Topological charge—Beyond its visual appearance, the global structure of a black hole shadow can be characterized by a topological charge [21]. For standard black holes, this charge is a robust invariant ($\delta = 1$), distinguishing them from objects like naked singularities which possess a different topology. Here, we demonstrate that the formation of a cusp fundamentally alters this invariant, thereby driving a genuine topological phase transition.

The topological charge is defined by the winding number of a tangential vector around the shadow boundary via the Gauss-Bonnet theorem [21]:

$$\delta = \frac{1}{2\pi} \left(\oint \frac{dl}{\mathcal{R}} + \sum_i \Delta\theta_i \right). \quad (4)$$

The first term measures the integral over the smooth parts of the boundary, where \mathcal{R} is the local radius of curvature. The second term accounts for a discrete sum over exterior angles $\Delta\theta_i$ at all non-differentiable cusp points.

For a smooth, non-cuspy shadow ($\eta > \eta_c$), the boundary is differentiable everywhere, and the second term vanishes. The integral can be evaluated by considering the slope of the boundary

$$\mathcal{F} = \frac{d\beta}{d\alpha}, \quad (5)$$

which is an important quantity and helpful in constructing the Maxwell equal law in the next section. By chang-

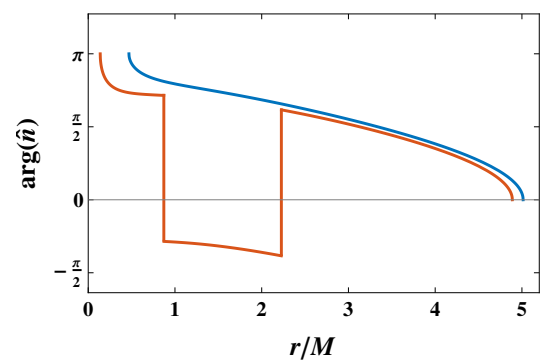


FIG. 2: Argument of the normal vector \hat{n} along the shadow boundary parameterized by r/M for $a/M = 2$. The deformation parameter $\eta/M^3 = 1.5$ and 0.5 are described by the top blue and bottom red curves, respectively. Note that the curve is segmented for $\eta/M^3 = 0.5$, and both the differences of the sudden change in the argument are $\Delta\theta = \pi$. As η/M^3 decreases, the length of the lower segment of the red curve increases.

ing the integration variable to the radius parameter r of the fundamental photon orbits and leveraging the shadow's \mathcal{Z}_2 symmetry, the charge simplifies to

$$\delta = \frac{1}{\pi} (\arctan \mathcal{F}(r_{min}) - \arctan \mathcal{F}(r_{max})), \quad (6)$$

where r_{min} and r_{max} correspond to the leftmost and rightmost points of the shadow, as indicated in Fig. 1. Considering that $\mathcal{F}(r_{max}) = -\infty$ and $\mathcal{F}(r_{min}) = +\infty$, one easily arrives the result

$$\delta = 1. \quad (7)$$

This confirms that the non-Kerr shadow, so long as it remains smooth, belongs to the same topological class as the Kerr shadow. This can also be obtained by the argument of the normal vector \hat{n} along the shadow boundary parameterized by r . Taking $\eta/M^3 = 1.5$ as an example (top blue curve in Fig. 2), where no cusp patterns are observed, it is evident that as r ranges from r_{max} to r_{min} , the argument progressively increases from 0 to π , yielding $\delta = \pi/\pi = 1$.

However, the topology changes dramatically in the presence of cusps (e.g. $\eta/M^3 = 0.5$). As shown in Fig. 2, the cusps introduce sharp, discontinuous jumps in the argument of the boundary's normal vector described by the bottom red curve. Each cusp contributes an angle jump of $\Delta\theta = -\pi$. Including these contributions and exploiting the \mathcal{Z}_2 symmetry the topological charge (6) for the cuspy shadow becomes

$$\delta = \frac{1}{\pi} (\pi + \Delta\theta_1 + \Delta\theta_2) = \frac{1}{\pi} (\pi - \pi - \pi) = -1. \quad (8)$$

This result is profound: the topological charge flips from $\delta = 1$ to $\delta = -1$. This is not a small perturbation but a fundamental change in the global properties of the

shadow. It rigorously proves that shadows with and without cusps belong to entirely different topological classes, with the cusp acting as topological genus.

Gravitational equal-area law—The self-intersecting boundary of a cuspy shadow is strikingly reminiscent of the swallow tail behavior of the free energy for a van der Waals fluid undergoing a liquid-gas phase transition. In thermodynamics, the unphysical, multi-valued region of the isotherm is resolved by the Maxwell equal-area law, which precisely determines the coexistence pressure. Here, we construct an analogous law to identify the self-intersection point of the shadow.

We can treat the shadow boundary as a thermodynamic-like curve in the (\mathcal{F}, α) plane, where \mathcal{F} , as defined in Eq. (5), serves as the variable conjugate to the celestial coordinate α . For a fixed black hole configuration (with constant a and η), the closed loop integral on the shadow's state space must vanish. At a self-intersection point, two different photon orbits (parameterized by r_1 and r_2) coincide at the same celestial coordinates (α_*, β_*) . The condition that the loop integral $\oint d\beta$ vanishes along a loop connecting these two points leads directly to our gravitational equal-area law:

$$\oint \mathcal{F} d\alpha = 0, \quad (9)$$

or equivalently

$$\int_{\mathcal{F}_1}^{\mathcal{F}_2} \alpha d\mathcal{F} = \alpha_*(\mathcal{F}_2 - \mathcal{F}_1), \quad (10)$$

where \mathcal{F}_2 and \mathcal{F}_1 correspond to the same α_* , a relationship linked to the self-intersection point that is under consideration for determination. This dictates that the self-intersection point α_* must be chosen such that it equalizes the two areas enclosed by the non-monotonic curve and a vertical line at α_* in the (\mathcal{F}, α) plane, as illustrated in Fig. 3.

We numerically verify this law for the KZ black hole with $a/M = 2$. As illustrated in Fig. 3, constant- η curves below the critical value ($\eta < \eta_c$) exhibit the characteristic non-monotonic behaviour required for a first-order-like phase transition. By applying our equal-area construction, we can precisely locate the self-intersection point. For $\eta/M^3 = 0.5$, the law uniquely identifies the intersection at $\alpha_* \approx 3.872$ with conjugate variable values $\mathcal{F}_1 = -0.0168743$ and $\mathcal{F}_2 = 0.839669$. This corresponds to two distinct fundamental photon orbits with radii $r_1/M \approx 3.164$ and $r_2/M \approx 0.642$, respectively. These values are in perfect agreement with direct numerical results, confirming the validity of our construction.

As η increases towards the critical value η_c , the enclosed area (see $\eta/M^3 = 0.6, 0.7$, and 0.8 in Fig. 3) gradually decreases and vanishes exactly at the critical point. This behavior is perfectly analogous to a thermodynamic system near its critical point. This establishes the equal-area law as a robust and fundamental tool for

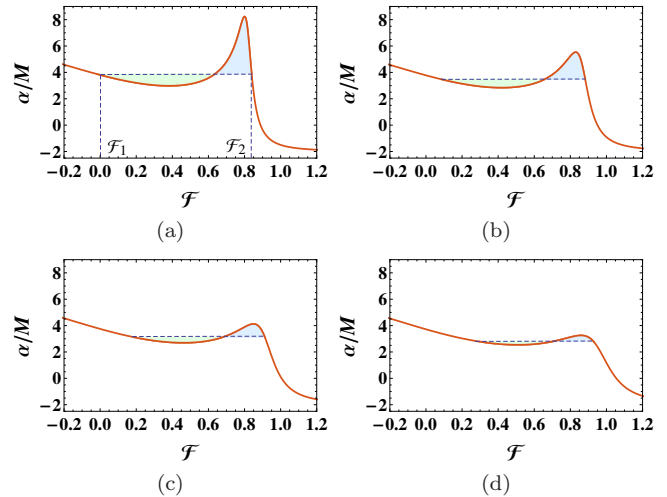


FIG. 3: Gravitational equal-area law for the cuspy black hole shadow with $a/M = 2$. (a) $\eta/M^3=0.5$. The two equal areas are each 3.316, with the slopes $\mathcal{F}_1=-0.0169$ and $\mathcal{F}_2=0.8397$. (b) $\eta/M^3=0.6$. The two equal areas are 2.755. (c) $\eta/M^3=0.7$. The two equal areas are 0.134. (d) $\eta/M^3=0.8$. The two equal areas are 0.064. The horizontal dashed lines are for $\alpha_*/M=3.872, 3.469, 3.109$, and 2.785 for (a)-(d), respectively.

analyzing the morphology of non-Kerr black hole shadows.

Critical phenomena—The transition from a smooth to a cuspy shadow is a critical phenomenon characterized by a non-analytic change. The critical point—the exact threshold where the cusps first appear—occurs when the two areas in our equal-area construction vanish. This corresponds to an inflection point in the (α, \mathcal{F}) plane, defined by the conditions:

$$\left(\frac{\partial \alpha}{\partial \mathcal{F}} \right)_{a,\eta} = 0, \quad \left(\frac{\partial^2 \alpha}{\partial \mathcal{F}^2} \right)_{a,\eta} = 0. \quad (11)$$

Taking $a/M = 2$, we identify the critical point as $\alpha_c/M = 2.088$ and $\eta_c/M^3 = 1.052$. Instances where $\alpha > \alpha_c$ or $\eta < \eta_c$ will manifest the cuspy shadow. By employing the equal-area law illustrated in Fig. 3, we can derive the respective values of \mathcal{F}_1 and \mathcal{F}_2 . These numerical outcomes are depicted in Fig. 4. As α and η approach their critical values, \mathcal{F}_1 increases while \mathcal{F}_2 decreases, indicating a reduction in the cuspy patterns. At the critical point, $\mathcal{F}_2 = \mathcal{F}_1$, and the cuspy patterns converge towards a point, beyond which the pattern completely disappears.

Near a critical point, physical systems often exhibit universal behavior characterized by critical exponents. Analogous with thermodynamic phase transitions [22, 23], we treat the difference between the self-intersecting branches, $\Delta\mathcal{F} = \mathcal{F}_2 - \mathcal{F}_1$, as the order parameter. This order parameter should scale as a power law with the

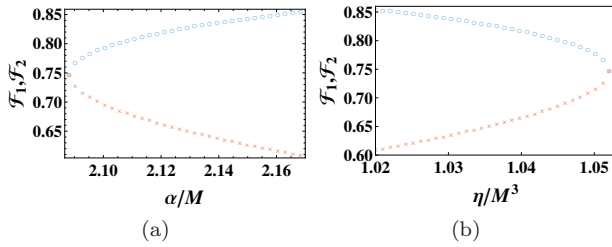


FIG. 4: Numerical results of \mathcal{F}_1 (bottom curves) and \mathcal{F}_2 (top curves) with $a/M = 2$ near the critical point. The critical value of \mathcal{F} is 0.747. (a) \mathcal{F} vs. α/M . The critical point is at $\alpha_c/M = 2.088$. (b) \mathcal{F} vs. η/M^3 . The critical point is at $\eta_c/M^3 = 1.052$.

distance from the critical point:

$$\Delta\mathcal{F} \sim \left(\frac{\alpha - \alpha_c}{M}\right)^{\zeta_1}, \quad (12)$$

$$\Delta\mathcal{F} \sim \left(\frac{\eta_c - \eta}{M^3}\right)^{\zeta_2} \quad (13)$$

with ζ_i defined as the respective critical exponents. To test this hypothesis, we numerically computed $\Delta\mathcal{F}$ as a function of $(\alpha - \alpha_c)$ or $(\eta_c - \eta)$ using our equal-area law. The results are shown on a log-log plot in Fig. 5. These data points fall perfectly on straight lines, and a linear fit yields $\zeta_1 = 0.495$ and $\zeta_2 = 0.496$. This alignment strongly supports the conclusion that the critical exponents are $\zeta_1 = \zeta_2 = \frac{1}{2}$.

We further confirm this by analyzing the behavior of the corresponding unstable fundamental photon orbits, r_1 and r_2 . The difference $\Delta r = r_2 - r_1$ also serves as an excellent order parameter. Power-law fits of Δr versus $(\alpha - \alpha_c)$ and $(\eta_c - \eta)$ yield critical exponents of 0.4999 and 0.5018, respectively.

Both calculations robustly yield a critical exponent of

$$\zeta = \frac{1}{2}. \quad (14)$$

This result is highly significant. A critical exponent of $1/2$ is the hallmark of the mean-field universality class (where the critical exponent $\beta = 1/2$), which describes a vast range of physical systems, from the Curie-Weiss model of magnetism to the van der Waals liquid-gas transition. Our results establish that cusp formation in a black hole shadow is not merely analogous to a thermodynamic phase transition—it is a direct manifestation of the same fundamental universality class.

Summary— We have established a new framework for understanding the shadows of non-Kerr black holes, revealing that cusp formation is not a simple morphological change but a true topological phase transition. By connecting strong-field gravitational lensing to the physics of topology and thermodynamical critical phenomena, we uncovered the fundamental principles governing these exotic shadow shapes.

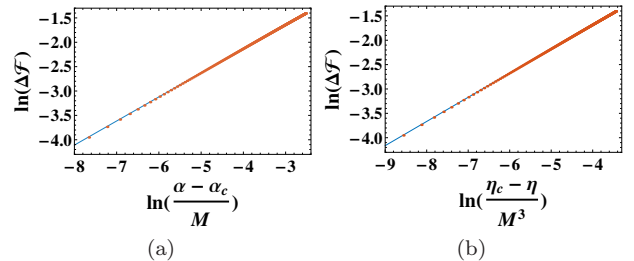


FIG. 5: Critical behavior of $\Delta\mathcal{F} = \mathcal{F}_2 - \mathcal{F}_1$ with $a/M = 2$. Dots represent numerical results, and blue lines correspond to fitting curves. (a) $\Delta\mathcal{F}$ vs. $\ln(\frac{\alpha - \alpha_c}{M})$. The slope of the blue line is 0.495. (b) $\Delta\mathcal{F}$ vs. $\ln(\frac{\eta_c - \eta}{M^3})$. The slope of the blue line is 0.496.

Our investigation yielded three key results. First, we proved that cuspy shadows are topologically distinct from their smooth counterparts, characterized by a topological charge of $\delta = -1$ in stark contrast to the $\delta = 1$ of Kerr-like shadows. Second, we introduced a novel gravitational equal-area law, analogous to Maxwell's construction in thermodynamics, which provides a robust and predictive tool for analyzing the shadow's structure. Finally, by treating the onset of cusp formation as a critical phenomenon, we identified a universal critical exponent of $\zeta = 1/2$. This finding rigorously places this gravitational system into the mean-field universality class, establishing a profound link between black hole optics and statistical mechanics.

These findings open several new avenues for both theory and observation. Black holes having only unstable fundamental photon orbits will have standard shadows, whereas cuspy shadows will appear once stable fundamental photon orbits become possible. Hence a cuspy shadow furnishes a test of the presence of stable fundamental photon orbits, a phenomenon we expect to hold beyond the KZ black holes we have considered here, but also for black holes with Proca hair, those embedded in dark matter halos, and other possible black objects [16–19]. Furthermore, the critical behavior we have identified suggests that near-threshold black holes could exhibit unique signatures, such as sharp changes in luminosity, which may be detectable with next-generation telescopes. Furthermore, the connection between stable fundamental photon orbits and accretion flow dynamics implies that these topological features could imprint discernible patterns on accretion disks. Our framework provides the necessary tools to model these effects, transforming the search for new physics from a hunt for subtle deviations into a targeted search for the distinct topological and critical phenomena revealed in this work.

Acknowledgements.— This work was supported by the National Natural Science Foundation of China (Grants No. 12475055, No. 12475056, No. 12247101) and by the Natural Science and Engineering Research Council of Canada.

[1] J. L. Synge, *The escape of photons from gravitationally intense stars*, MNRAS, **131**, 463 (1966).

[2] J. P. Luminet, *Image of a spherical black hole with thin accretion disk*, A. A, **75**, 228 (1979).

[3] J. M. Bardeen, *Timelike and null geodesics in the Kerr metric*, Les Astres Occlus, (1973).

[4] S. Chandrasekhar, *The Mathematical Theory of Black Holes*, Oxford University Press, New York, (1992).

[5] K. Hioki and K. I. Maeda, *Measurement of the Kerr Spin Parameter by Observation of a Compact Object's Shadow*, Phys. Rev. D **80**, 024042 (2009), [arXiv:0904.3575 [astro-ph.HE]].

[6] The Event Horizon Telescope Collaboration, *First M87 Event Horizon Telescope Results. I. The Shadow of the Supermassive Black Hole*, Astrophys. J. Lett. **875**, L1 (2019), [arXiv:1906.11238 [astro-ph.GA]].

[7] The Event Horizon Telescope Collaboration, *First Sagittarius A* Event Horizon Telescope Results. I. The Shadow of the Supermassive Black Hole in the Center of the Milky Way*, Astrophys. J. Lett. **930**, L12 (2022), [arXiv:2311.08680 [astro-ph.HE]].

[8] The Event Horizon Telescope Collaboration, *Constraints on black-hole charges with the 2017 EHT observations of M87**, Phys. Rev. D **103**, 104047 (2021), [arXiv:2105.09343 [gr-qc]].

[9] S. E. Gralla, D. E. Holz, and R. M. Wald, *Black Hole Shadows, Photon Rings, and Lensing Rings*, Phys. Rev. D **100**, 024018 (2019), [arXiv:1906.00873 [astro-ph.HE]].

[10] P. V. P. Cunha and C. A. R. Herdeiro, *Shadows and strong gravitational lensing: a brief review*, Gen. Rel. Grav. **50**, 42 (2018), [arXiv:1801.00860 [gr-qc]].

[11] V. Perlick and O. Yu. Tsupko, *Calculating black hole shadows: Review of analytical studies*, Physics Reports, **947**, 1 (2022), [arXiv:2105.07101 [gr-qc]].

[12] P. V. P. Cunha, C. A. R. Herdeiro, E. Radu, and H. F. Runarsson, *Shadows of Kerr black holes with scalar hair*, Phys. Rev. Lett. **115**, 211102 (2015), [arXiv:1509.00021 [gr-qc]].

[13] X.-M. Kuang, Y. Meng, E. Papantonopoulos, and X.-J. Wang, *Using the shadow of a black hole to examine the energy exchange between axion matter and a rotating black hole*, Phys. Rev. D **110**, L061503 (2024), [arXiv:2406.11932 [gr-qc]].

[14] Y. Huang, D.-J. Liu, and H. Zhang, *Shadows of rotating black holes with parity-odd scalar hair*, J. High Energy Phys. **11**, 027 (2025), [arXiv:2507.04761 [gr-qc]].

[15] P. V. P. Cunha, *Backreaction of perturbations around a stable Light Ring*, JCAP **05**, 083 (2025), [arXiv:2503.00117 [gr-qc]].

[16] P. V. P. Cunha, C. A.R. Herdeiro, and E. Radu, *Fundamental photon orbits: black hole shadows and spacetime instabilities*, Phys. Rev. D **96**, 024039 (2017), [arXiv:1705.05461 [gr-qc]].

[17] M. Wang, S. Chen, and J. Jing, *Shadow casted by a Konoplya-Zhidenko rotating non-Kerr black hole*, JCAP **10**, 051 (2017), [arXiv:1707.09451 [gr-qc]].

[18] W.-L. Qian, S. Chen, C.-G. Shao, B. Wang, and R.-H. Yue, *Cuspy and fractured black hole shadows in a toy model with axisymmetry*, Eur. Phys. J. C **82**, 91 (2022), [arXiv:2102.03820 [gr-qc]].

[19] C.-Y. Chen, C.-M. Chen, and N. Ohta, *Shadow of black holes with consistent thermodynamics*, [arXiv:2510.00708 [gr-qc]].

[20] R. Konoplya and A. Zhidenko, *Detection of gravitational waves from black holes: Is there a window for alternative theories?*, Phys. Lett. B **756**, 350 (2016), [arXiv:1602.04738 [gr-qc]].

[21] S.-W. Wei, Y.-X. Liu, and R. B. Mann, *Intrinsic curvature and topology of shadows in Kerr spacetime*, Phys. Rev. D **99**, 041303 (2019), [arXiv:1811.00047 [gr-qc]].

[22] D. Kubiznak and R. B. Mann, *P – V criticality of charged AdS black holes*, JHEP **1207**, 033 (2012), [arXiv:1205.0559 [hep-th]].

[23] S.-W. Wei and Y.-X. Liu, *Clapeyron equations and fitting formula of the coexistence curve in the extended phase space of charged AdS black holes*, Phys. Rev. D **91**, 044018 (2015), [arXiv:1411.5749 [hep-th]].